

# COMPENSATION FOR DISTORTION OF DYNAMIC SENSOR DATA USING RECEPTANCE COUPLING

Tony L. Schmitz

University of Florida, Department of Mechanical and Aerospace Engineering, Gainesville, FL 32611

## 1. INTRODUCTION

Sensors can be used to record a number of phenomena on mechanical structures. Applications of this sensor data include process metrology, condition-based maintenance, general fault diagnosis, and non-destructive evaluation, for example. In many cases, the recorded information is dynamic in nature and minimum requirements for the sensor frequency response, in addition to accuracy, resolution, and durability, are required. However, even if a satisfactory sensor (or sensors) is selected, if the sensor cannot be placed directly at the point of interest, the structural dynamics between the two locations can adversely affect the measured signal through both scaling errors and distortion of the frequency content. In this work, a unified mathematical approach for assembly dynamics prediction using receptance coupling techniques is presented. The predicted models can be applied to remove the effects of structural dynamics on the measured data and select high signal-to-noise ratio sensor mounting locations.

## 2. METHOD DESCRIPTION

### 2.1 Compensation for non-ideal sensor location

Substructure analysis, or component mode synthesis, methods have been used for several decades to predict the dynamic response of assemblies using measurements and/or models of the individual components, or substructures. These components can be represented by spatial mass, stiffness, and damping data; modal data; or receptances [e.g., 1-7]. The latter representation is generally preferred in situations where the assembly receptances are the desired analysis output, as is the case here. This research builds on the previous receptance coupling work by including both translational and rotational degrees of freedom and applying the assembly dynamics models to sensor data compensation.

To demonstrate the method, consider the prismatic cantilever beam-cylinder assembly shown in Fig. 1, where a harmonic force,  $F_1(t)$ , is applied to the free end of the cylinder, coordinate  $X_1$ , and the resulting displacement  $X_1(t)$  is to be determined. The preferred solution is to place an appropriate linear transducer at this location and record the required displacement directly. However, if access to the cylinder is obstructed, it may be required to place the sensor remotely at coordinate  $X_2$ , for example. Due to the change in cross-section and increased stiffness, there is reduced sensitivity to the  $X_1$  vibrations for  $X_2$  measurements. Additionally, the vibration measured at

$X_2$  can be influenced by the assembly's structural response between coordinates  $X_1$  and  $X_2$ . Finally,  $X_2$  may be located at a node of one of the assembly mode shapes.

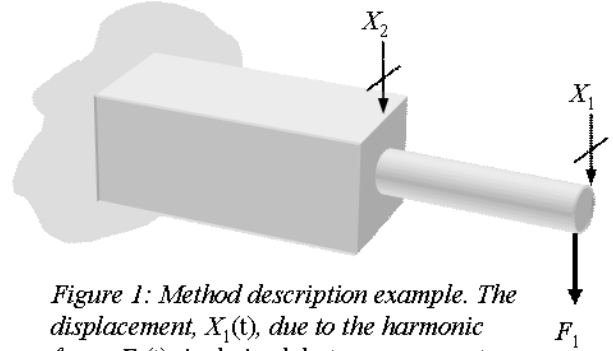


*Figure 1: Method description example. The displacement,  $X_1(t)$ , due to the harmonic force,  $F_1(t)$ , is desired, but measurements can only be performed at coordinate  $X_2$ .*

In order to determine  $X_1(t)$  from  $X_2$  measurements, the following three steps are carried out.

1. Measure the time-domain response  $X_2(t)$  and Fourier transform to obtain the frequency-domain result  $X_2(\omega)$ .
2. The relationship between  $X_2(\omega)$  and  $F_1(\omega)$  can be expressed by:

$$X_2(\omega) = H_{21}F_1(\omega), \quad (1)$$

where  $H_{21}$  is the assembly displacement-to-force cross receptance between coordinates  $X_2$  and  $X_1$ . Solving for  $F_1$  gives  $F_1(\omega) = H_{21}^{-1}X_2(\omega)$ . This result can be substituted in the equation relating  $X_1(\omega)$  and  $F_1(\omega)$  to obtain:

$$X_1(\omega) = H_{11}F_1(\omega) = H_{11}H_{21}^{-1}X_2(\omega), \quad (2)$$

where  $H_{11}$  is the assembly displacement-to-force direct receptance at coordinate  $X_1$ .

3. Inverse Fourier transform  $X_1(\omega)$  to obtain  $X_1(t)$ . This result now provides the required information and removes the influence of the structural dynamics between  $X_1$  and  $X_2$ . Note that the time-domain force,  $F_1(t)$ , is also available by inverse Fourier transforming  $F_1(\omega)$ .

To carry out these steps, the assembly displacement-to-force receptances  $H_{11}(\omega)$  and  $H_{21}(\omega)$  must be known. The straightforward approach is to measure them directly using some external mechanical excitation, such as a hammer or shaker, and record the response using a

linear transducer, e.g., accelerometer, vibrometer, or displacement probe. However, there may be situations where either the measurements are difficult to carry out (due to mechanical obstruction) or the assembly changes regularly (for example, multiple tools and holders may be used in a single milling spindle [8-13]). In these cases, an accurate model is required.

One choice for developing the model is finite element analysis, or FEA, which can provide quality estimates of natural frequency and mode shapes. A current limitation of this method, however, is the treatment of joints, particularly the energy dissipation, or damping, at contact interfaces. This is critically important in the sensor data compensation proposed here because properly scaled assembly receptances, which depend strongly on damping, are required. In many cases, an FEA *a priori* prediction of assembly dynamics from design drawings is difficult or impossible. As an alternative, receptance coupling offers a hybrid method where measured receptances can be coupled to modeled receptances through appropriate connections, which can include both finite stiffness and non-zero damping. The general approach is to measure those components with difficult-to-predict behavior and model those components that are more suited to successful prediction using modeling techniques.

To determine the dynamics for the assembly shown in Fig. 1 by receptance coupling, several considerations must be made. First, only displacement-to-force receptances,  $H_{ij}$ , have been discussed so far. However, if accurate assembly predictions are to be made, all four bending receptances must be included in the component descriptions (i.e., displacement-to-force,  $H_{ij}$ , displacement-to-moment,  $L_{ij}$ , rotation-to-force,  $N_{ij}$ , and rotation-to-moment,  $P_{ij}$ ). Second, the compatibility conditions at the component interfaces must be selected; these can be rigid, flexible with no damping, or flexible with damping. Third, the component receptances must be determined. If measurements are completed, care must be taken to accurately record all four receptances with adequate bandwidth and resolution. The steps required to predict the Fig. 1 assembly receptances follow.

1. Define the components and coordinates for the model. In this simple example, two components can be defined: a prismatic cantilever and free-free cylinder (see Fig. 2).

2. Describe the component receptances. Both measurements and models can be used. For the models, the closed-form receptance functions presented by Bishop and Johnson [1] for the analysis of flexural vibrations of uniform Euler-Bernoulli beams with free, fixed, sliding, and pinned boundary conditions are applied here. For example, the direct and cross receptances for the free-free cylinder due to the component forces  $f_1(t)$  and  $f_2(t)$ , applied at coordinates

$x_1(t)$  and  $x_2(t)$ , respectively, and moments  $m_1(t)$  and  $m_2(t)$ , applied at  $\theta_1(t)$  and  $\theta_2(t)$ , respectively, are compactly represented in Eq. (3) (lower case notation is used to designate component variables).

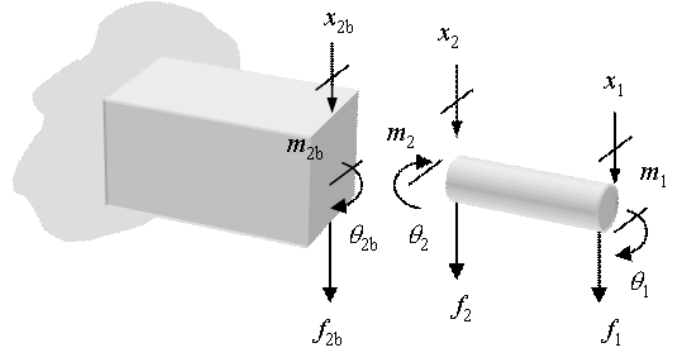


Figure 2: Components for the receptance coupling example. Two components are connected to form the assembly.

$$\begin{aligned} \begin{Bmatrix} x_1 \\ \theta_1 \end{Bmatrix} &= \begin{bmatrix} h_{11} & l_{11} \\ n_{11} & p_{11} \end{bmatrix} \begin{Bmatrix} f_1 \\ m_1 \end{Bmatrix} \quad \text{or} \quad \{u_1\} = [R_{11}]\{q_1\}, \\ \begin{Bmatrix} x_2 \\ \theta_2 \end{Bmatrix} &= \begin{bmatrix} h_{22} & l_{22} \\ n_{22} & p_{22} \end{bmatrix} \begin{Bmatrix} f_2 \\ m_2 \end{Bmatrix} \quad \text{or} \quad \{u_2\} = [R_{22}]\{q_2\} \quad (3) \\ \begin{Bmatrix} x_1 \\ \theta_1 \end{Bmatrix} &= \begin{bmatrix} h_{12} & l_{12} \\ n_{12} & p_{12} \end{bmatrix} \begin{Bmatrix} f_2 \\ m_2 \end{Bmatrix} \quad \text{or} \quad \{u_1\} = [R_{12}]\{q_2\}, \\ \begin{Bmatrix} x_2 \\ \theta_2 \end{Bmatrix} &= \begin{bmatrix} h_{21} & l_{21} \\ n_{21} & p_{21} \end{bmatrix} \begin{Bmatrix} f_1 \\ m_1 \end{Bmatrix} \quad \text{or} \quad \{u_2\} = [R_{21}]\{q_1\} \end{aligned}$$

where  $R_{ij}$  is the generalized receptance matrix that describes both translational and rotational component behavior [11]. The individual entries in these matrices depend on the boundary conditions and include contributions from both the rigid body (if applicable) and flexural modes. For example, at the right end of the free-free cylinder, the  $R_{11}$  matrix terms are:

$$h_{11}(\omega) = \frac{x_1}{f_1} = \frac{-(\cos \lambda L \sinh \lambda L - \sin \lambda L \cosh \lambda L)}{EI(1+\eta)\lambda^3(\cos \lambda L \cosh \lambda L - 1)} \quad (4)$$

$$l_{11}(\omega) = \frac{x_1}{m_1} = n_{11}(\omega) = \frac{\theta_1}{f_1} = \frac{-(\sin \lambda L \sinh \lambda L)}{EI(1+\eta)\lambda^2(\cos \lambda L \cosh \lambda L - 1)}$$

$$p_{11}(\omega) = \frac{\theta_1}{m_1} = \frac{(\cos \lambda L \sinh \lambda L + \sin \lambda L \cosh \lambda L)}{EI(1+\eta)\lambda(\cos \lambda L \cosh \lambda L - 1)},$$

where  $\lambda = \left( \frac{m\omega^2}{LEI(1+i\eta)} \right)^{\frac{1}{4}}$ ,  $m$  is the beam mass (kg),  $\omega$  is the frequency (rad/s),  $L$  is the beam length (m),  $E$  is the elastic modulus (N/m<sup>2</sup>),  $I$  is the 2<sup>nd</sup> area moment of inertia

(m<sup>4</sup>), and  $\eta$  is the structural damping factor (unitless). [Damping was not included in reference [1], but has been added as part of this analysis.] These receptances can be used to couple components at their end points in order to determine assembly dynamics.

3. Based on the selected model from step 1, express the assembly receptances (see Eq. (5), where upper case notation is used to designate assembly variables). These receptances are determined by first writing the component displacements/ rotations as shown in Eq. (6).

$$\begin{Bmatrix} U_1 \\ U_2 \end{Bmatrix} = \begin{bmatrix} G_{11} & G_{12} \\ G_{21} & G_{22} \end{bmatrix} \begin{Bmatrix} Q_1 \\ Q_2 \end{Bmatrix}, \text{ where} \\ U_i = \begin{Bmatrix} X_i \\ \Theta_i \end{Bmatrix}, \quad G_{ij} = \begin{bmatrix} H_{ij} & L_{ij} \\ N_{ij} & P_{ij} \end{bmatrix}, \text{ and} \quad Q_i = \begin{Bmatrix} F_i \\ M_i \end{Bmatrix} \quad (5)$$

$$\begin{aligned} u_1 &= R_{11}q_1 + R_{12}q_2 & u_2 &= R_{21}q_1 + R_{22}q_2 \\ u_{2b} &= R_{2b2b}q_{2b} \end{aligned} \quad (6)$$

If the prismatic cantilever beam-cylinder assembly is considered to be a solid body with the cylindrical portion formed by turning one end of the beam down to its final diameter, for example, a rigid connection is applied at the component interface and the compatibility conditions are:

$$u_2 - u_{2b} = 0 \text{ and } u_i = U_i, i = 1 \text{ to } 2, \quad (7)$$

where the latter expression specifies that the component and assembly coordinates are defined at the same spatial positions. The equilibrium conditions vary with the external force/moment location. To determine the first column of the assembly receptance matrix in Eq. (5),  $Q_1$  is applied to coordinate  $U_1$ . In this case, the equilibrium conditions are:

$$q_2 + q_{2b} = 0 \text{ and } q_1 = Q_1. \quad (8)$$

Substitution of the component displacements/rotations and equilibrium conditions into the compatibility conditions yields  $q_2$  (see Eq. (9)). The expression for  $G_{11}$  is then given by Eq. (10). The other first column receptance is determined in a similar manner;  $G_{21}$  is shown in Eq. (11). To find the receptances in the second column,  $Q_2$  must be applied to  $U_2$ .

$$q_2 = -(R_{22} + R_{2b2b})^{-1} R_{21} Q_1 \quad (9)$$

Equations (10) and (11) contain the assembly receptances required to solve Eq. (2) for  $X_1(t)$  from sensor data recorded at  $X_2$ . In this example, these receptances were developed analytically using material properties and component geometry. However, any of the component response terms could also be replaced by

actual measurement data (no curve fitting or modal parameter estimation is required).

$$\begin{aligned} G_{11} &= \frac{U_1}{Q_1} = \frac{u_1}{Q_1} = \frac{R_{11}q_1 + R_{12}q_2}{Q_1} = \\ R_{11} - R_{12}(R_{22} + R_{2b2b})^{-1} R_{21} &= \begin{bmatrix} H_{11} & L_{11} \\ N_{11} & P_{11} \end{bmatrix} \end{aligned} \quad (10)$$

$$\begin{aligned} G_{21} &= \frac{U_2}{Q_1} = \frac{u_2}{Q_1} = \frac{R_{21}q_1 + R_{22}q_2}{Q_1} = \\ R_{21} - R_{22}(R_{22} + R_{2b2b})^{-1} R_{21} &= \begin{bmatrix} H_{21} & L_{21} \\ N_{21} & P_{21} \end{bmatrix} \end{aligned} \quad (11)$$

## 2.2 Sensor location selection for high signal-to-noise

The receptance coupling approach described in the previous section can also be used to predict assembly mode shapes and, therefore, enable the selection of sensor locations with improved signal-to-noise ratios. Again considering the assembly in Fig. 1, the previous two-coordinate model is most likely insufficient to generate usable mode shapes. However, any number of coordinates can be added to improve the mode shapes' spatial resolution (within the limitations of Euler-Bernoulli beam theory). The model is redefined in Fig. 3 to include seven assembly coordinates, for example.

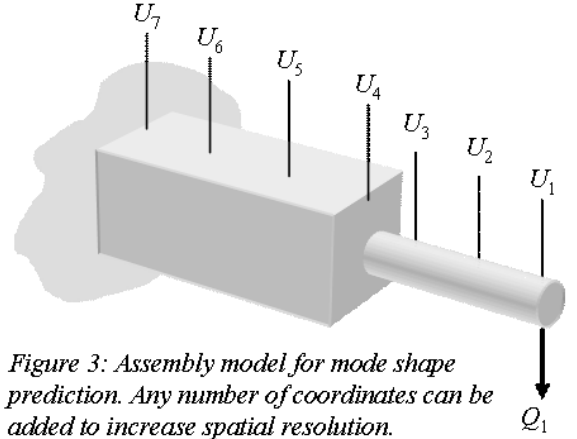


*Figure 3: Assembly model for mode shape prediction. Any number of coordinates can be added to increase spatial resolution.*

For this model, the assembly receptance matrix (Eq. (5)) is rewritten as shown in Eq. (12). To determine the 49  $G_{ij}$  entries, step 3 from the previous section is repeated multiple times for each column. For example, to determine the first column mode shapes,  $Q_1$  is applied to  $U_1$  as shown in Fig. 3.

The  $G_{11}$  and  $G_{21}$  terms are again calculated using Eqs. (10) and (11). However, the assembly is now sectioned at coordinate  $U_2$  to define the two components. To find  $G_{31}$ , the assembly is sectioned at  $U_3$  and the resulting equation is  $G_{31} = R_{31} - R_{33}(R_{33} + R_{3b3b})^{-1} R_{31}$ . The recursive pattern can be observed to find the remaining terms in the column.

$$\begin{Bmatrix} U_1 \\ U_2 \\ \vdots \\ U_7 \end{Bmatrix} = \begin{bmatrix} G_{11} & G_{12} & \cdots & G_{17} \\ G_{21} & G_{22} & \cdots & G_{27} \\ \vdots & \vdots & \ddots & \vdots \\ G_{71} & G_{72} & \cdots & G_{77} \end{bmatrix} \begin{Bmatrix} Q_1 \\ Q_2 \\ \vdots \\ Q_7 \end{Bmatrix} \quad (12)$$

Note that this result differs from traditional modal analysis where the number of natural frequencies and mode shapes must be equal to the number of model spatial coordinates in order to obtain square matrices. In Eq. (14), all 49 entries in the  $G_{ij}$  matrix are 2 by 2 by  $N$  matrices, where  $N$  is the number of points in the frequency vector,  $\omega$ . Each of the receptances in these matrices includes all modes within the frequency range of interest.

### 3. EXPERIMENTAL EVALUATION

To verify the receptance coupling approach, frequency response measurements were carried out on a 827.9 mm x 76.2 mm x 16.1 mm plastic beam using a small impact hammer (PCB 086D80) to excite the beam and low mass accelerometer (PCB 352B10) to record the response [14]. Free-free boundary conditions were approximated by suspending the beam vertically from a thin flexible wire (a 2 mm diameter hole was drilled at one end). The receptance coupling model of the constant cross-section prismatic beam was verified by measuring the direct frequency response function (FRF) at the ‘free’ end of the beam (away from the wire suspension) and comparing to the predicted response. The predicted and measured direct FRF are shown in Fig. 5. To populate the receptance model, the beam mass (944.3 g) and dimensions were recorded and the 2<sup>nd</sup> area moment of inertia was calculated. The modulus and structural damping factor were considered free parameters to enable a good fit between the model and data ( $E = 1.37 \times 10^9$  N/m<sup>2</sup> and  $\eta = 0.035$ ).

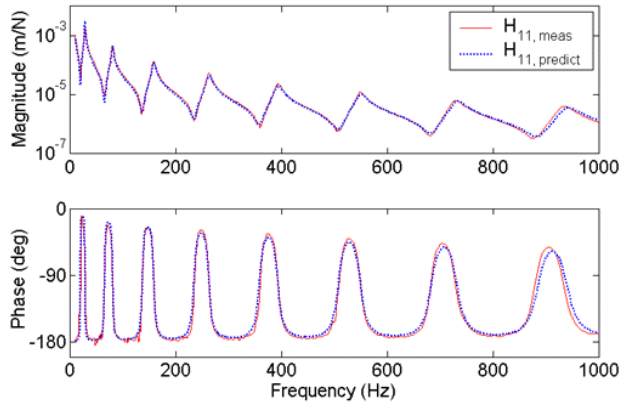


Figure 5: Measurement and model of plastic beam.

Once the beam model was established, cross FRF measurements were completed and compared to the cross receptances determined according to the approach described in Section 2.2. The analytical mode shapes are

compared to experimental results for the first three free-free bending modes in Fig. 6. In each case, the mode shape maximum amplitude was normalized to one.

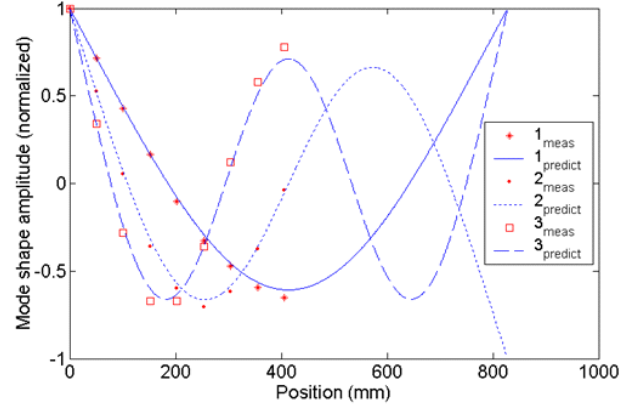


Figure 6: Mode shape predictions and measurements (first three mode shapes shown).

#### 3.1 Force prediction using acceleration data

As described in Section 2.1, the externally applied force can be determined from the measured response and system FRF model. To verify this approach experimentally, the suspended plastic beam was excited at its ‘free’ end using the impact hammer and the response was measured at the same location using the accelerometer. Both signals were analog low-pass filtered with a cutoff frequency of 1 kHz prior to digital sampling at 50 kHz for 2 sec. The measured acceleration,  $a_i(t)$ , was then Fourier transformed and pre-multiplied by the inverted direct accelerance, equal to the product of  $-\omega^2$  and the modeled direct receptance  $H_{11}(\omega)^{-1}$  (see Fig. 5), to find the frequency domain force,  $F_i(\omega) = (-\omega^2 \cdot H_{11})^{-1} A_i(\omega)$ . This result was then inverse Fourier transformed and compared to the input force due to the hammer impact. The force results and measured acceleration are shown in Fig. 7. The reader may note that the ringing in the hammer force is due to the analog low pass filtering.

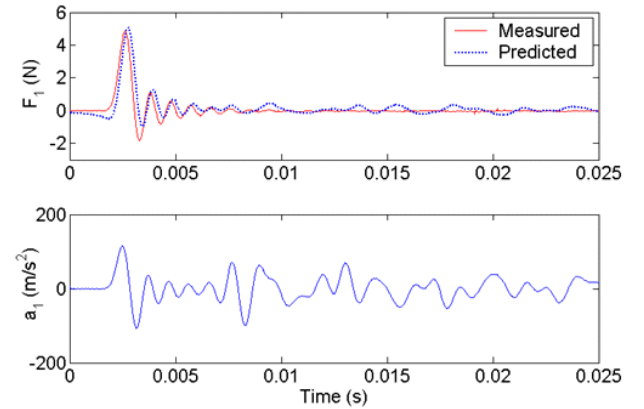


Figure 7: (Top panel) Measured and predicted forces; (bottom panel) acceleration response to  $F_1$  force input.

### 3.2 Correction for accelerometer placement

The exercise in Section 3.1 was repeated, except the accelerometer was not placed at the hammer input location. In this case, the hammer impact occurred 254 mm from the beam ‘free’ end. If this position is referred to as  $X_2$ , then the receptance  $H_{12}(\omega)$  can be used to determine the force,  $F_2(\omega) = (-\omega^2 \cdot H_{12})^{-1} A_1(\omega)$ . The  $H_{12}(\omega)$  receptance is found by artificially separating the beam into two components at  $X_2$  and then joining the components as described in Section 2.2. See Eq. (13), where the  $R_{12}$  and  $R_{22}$  cross and direct component receptances are determined using a 254 mm beam length, while the  $R_{2b2b}$  direct receptances are calculated using a beam length of  $(827.9-254) = 573.9$  mm. See Fig. 8. Note that incorrect results are obtained if only the displacement-to-force receptances are used, i.e.,  $H_{12} = h_{12}(h_{22} + h_{2b2b})^{-1} h_{2b2b}$ .

$$G_{12} = R_{12}(R_{22} + R_{2b2b})^{-1} R_{2b2b} = \begin{bmatrix} H_{12} & L_{12} \\ N_{12} & P_{12} \end{bmatrix} \quad (13)$$

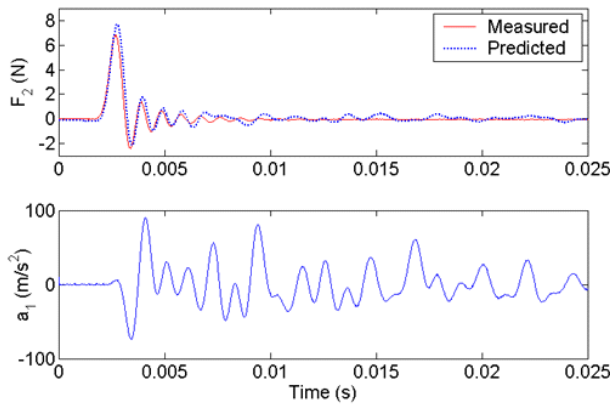


Figure 8: (Top panel) Measured and predicted forces; (bottom panel) acceleration response to  $F_2$  force input.

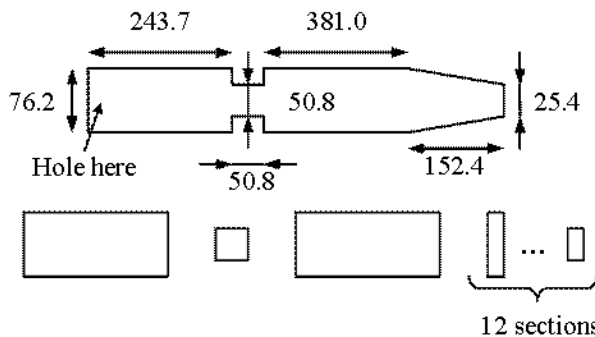


Figure 9: Modified beam model composed of 15 rigidly coupled sections (all dimensions in mm).

### 3.3 Modified beam geometry

For the next experiments, the beam geometry was modified by cutting away portions near the beam middle and tapering the beam ‘free’ end (Fig. 9). Using the

previous modulus, density, and structural damping values, the modified beam model was produced by rigidly coupling the 15 constant geometry sections shown in Fig. 9. The measured and predicted direct receptance at the ‘free’ tapered end are shown in Fig. 10. Reasonable agreement is seen, but the predicted natural frequencies for the higher order modes are increasingly too large.

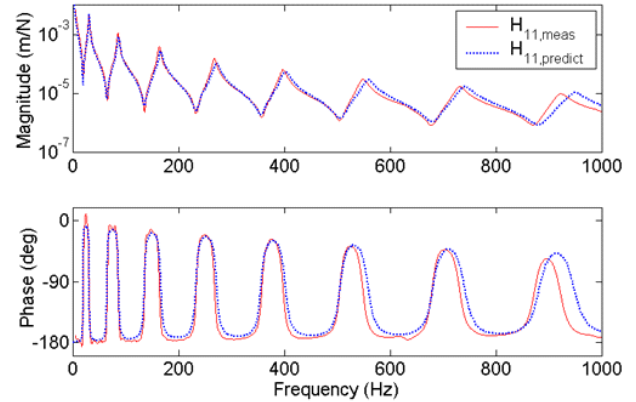


Figure 10: Measurement and model for modified plastic beam for direct receptance.

The force input was again reconstructed using accelerometer measurements at the tapered end and hammer impacts at: 1) the tapered end; and 2) 406.4 mm from the ‘free’ end, in conjunction with the corresponding model receptances. The measured and predicted cross receptance at the 406.4 mm location are provided in Fig. 11. The model divergence at higher frequencies is again observed.

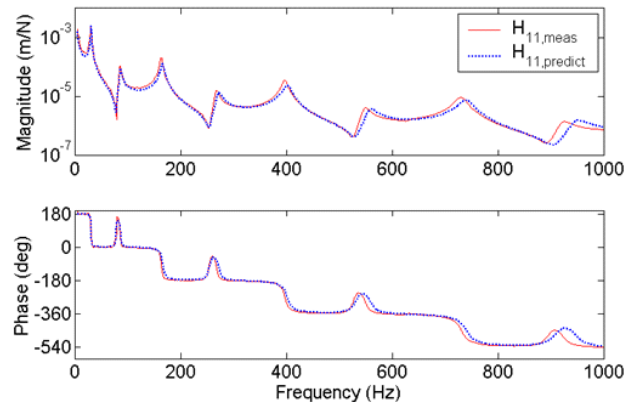


Figure 11: Measurement and model of modified plastic beam for cross receptance at 406.4 mm.

The measured and predicted force signals for the modified beam are shown in Figs. 12 and 13. Figure 12 shows the results for the force input at the beam tapered end, while Fig. 13 displays the results for hammer excitation 406.4 mm from the ‘free’ end. In both cases, additional content is seen in the predicted signal after the initial hammer impact. This extra (incorrect) force is due to the slight mismatch in natural frequencies between the model and actual beam. However, the

reconstructed forces still provide reasonable representations of the actual impacts.

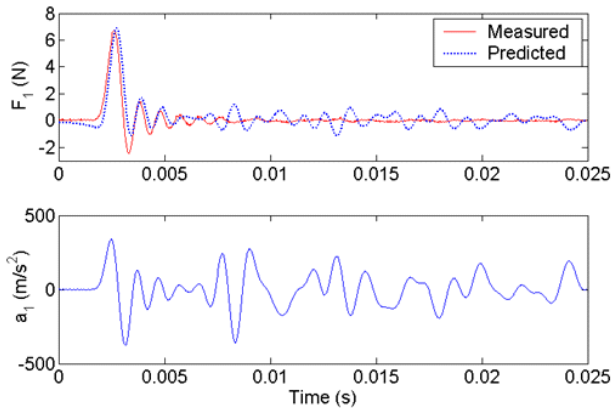


Figure 12: (Top panel) Measured and predicted forces; (bottom panel) acceleration response to  $F_1$  force input.

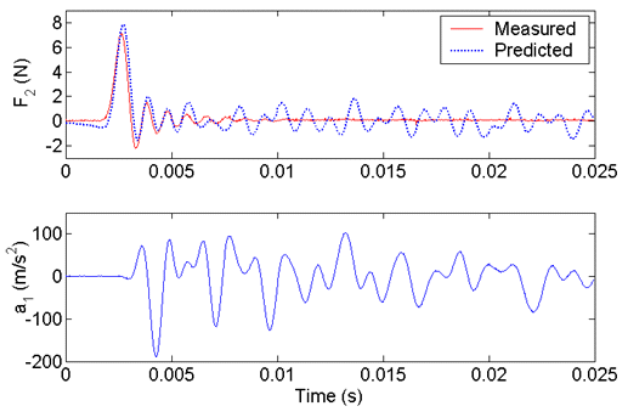


Figure 13: (Top panel) measured and predicted forces; (bottom panel) acceleration response to  $F_2$  force input.

#### 4. CONCLUSIONS

This paper describes the use of receptance coupling techniques to build dynamic models of assemblies in order to compensate for scaling and frequency distortion errors arising from non-ideal sensor placement on mechanical structures. The receptance coupling equations provided here include both translational and rotational degrees of freedom, as well as the potential for non-rigid connections between substructures.

Experimental results are provided for a plastic prismatic beam and it is shown that force signals can be recovered from acceleration measurements at: 1) the force input position; and 2) other locations. An impact force was applied so that a broad range of structural modes would be excited simultaneously and, therefore, provide a rigorous test for the approach. Experimental results are also shown for a modified beam geometry, where the mechanical properties determined from a fit to the direct displacement-to-force receptance at the end of the free-free original beam are used to develop a receptance coupling model for the new beam geometry.

Measurements and predictions are shown for both direct and cross receptances. Force reconstruction from accelerometer data, again using both direct and cross model receptances, is also provided.

#### 5. ACKNOWLEDGMENTS

The author gratefully acknowledges partial financial support for this research from the National Science Foundation (DMI-0238019) and Office of Naval Research (2003 Young Investigator Program). The author also thanks G. S. Duncan for contributions to this work.

#### 6. REFERENCES

1. Bishop, R.E.D. and Johnson, D.C., 1960, *The Mechanics of Vibration*, Cambridge University Press, Cambridge.
2. Hurty, W.C., 1965, Dynamic Analysis of Structural Systems using Component Modes. *AIAA Journal* 3/4: 678-685.
3. Klosterman, A.L., and Lemon, J.R., 1969, Building Block Approach to Structural Dynamics, *American Society of Mechanical Engineering Annual Vibration Conference*, publication VIBR-30.
4. Jetmundsen, B., Bielawa, R.L., and Flannelly, W.G., 1988, Generalized Frequency Domain Substructure Synthesis. *Journal of the American Helicopter Society* 33: 55-64.
5. Ren, Y. and Beards, C.F., 1995, On Substructure Synthesis with FRF Data, *Journal of Sound and Vibration* 185: 845-866.
6. Ewins, D.J., 2000, *Modal Testing: Theory, Practice and Application*, 2<sup>nd</sup> Edition, Research Studies Press, Philadelphia, PA.
7. Lui, W. and Ewins, D.J., 2002, Substructure Synthesis via Elastic Media, *Journal of Sound and Vibration* 257/2: 361-379.
8. Schmitz, T.L. and Donaldson, R., 2000, Predicting High-Speed Machining Dynamics by Substructure Analysis, *Annals of the CIRP* 49/1: 303-308.
9. Schmitz, T.L., Davies, M.A., and Kennedy, M., 2001, Tool Point Frequency Response Prediction for High-Speed Machining by RCSA, *ASME Journal of Manufacturing Science and Engineering* 123: 700-707.
10. Schmitz, T.L., Davies, M.A., Medicus, K., and Snyder, J., 2001, Improving High-Speed Machining Material Removal Rates by Rapid Dynamic Analysis, *Annals of the CIRP* 50/1: 263-268.
11. Park, S.S., Altintas, Y., and Movahhedy, M., 2003, Receptance Coupling for End Mills, *International Journal of Machine Tools and Manufacture*, 43: 889-896.
12. Yigit, A.S. and Ulsoy, A.G., 2002, Dynamic Stiffness Evaluation for Reconfigurable Machine Tools including Weakly Non-linear Joint Characteristics, Proceedings of the I MECH E Part B, *Journal of Engineering Manufacture*, 216/1: 87-101.
13. Schmitz, T. and Burns, T., 2003, Receptance Coupling for High-Speed Machining Dynamics Prediction, *Proceedings of the 21<sup>st</sup> International Modal Analysis Conference*, February 3-6, Kissimmee, FL (on CD).
14. Equipment manufacturers are specified for completeness. This does not imply endorsement by the author or the University of Florida.